Proceedings of the Project Review, Geo-Mathematical Imaging Group (Purdue University, West Lafayette IN), Vol. 1 (2009) pp. 71-90.

ILLUMINATION ANALYSIS OF WAVE-EQUATION IMAGING WITH "CURVELETS"

SHEN WANG *, MAARTEN V. DE HOOP †, AND BJØRN URSIN ‡

Abstract. We present a comprehensive framework for wave-equation illumination analysis and introduce a target-oriented illumination correction that simultaneously accounts for limited acquisition aperture and, locally, compensates for the so-called normal operator in inverse scattering to yield a "true-amplitude" image of reflectivity or reflection coefficient, while minimizing (orientation dependent) phase distortions and artifacts. The corrections are nested while the most significant correction is typically the one associated with the limited acquisition aperture. To carry out the analysis we make use of higher-dimensional "curvelets", which provide the means of extracting directional information, and introduce associated matrix representations for the component operators, including the tapers associated with the acquisition aperture, that make up wave-equation migration; we essentially exploit the properties of these matrices. Curvelets can be viewed as "fat", optimally localized plane waves and hence form a natural candidate to generalize geophysical diffraction tomography, which is at the basis of our approach. Our approach admits the formation of caustics and, hence, is valid in complex velocity models, though these need to be known for the illumination compensation to be effective.

1. Introduction. It remains a challenge to generate images that admit a quantitative interpretation in regions of complex geology, even if an accurate velocity or background model has been obtained. Typically, limited acquisition aperture gives rise to – dip dependent – image amplitude variations, and phase distortions and artifacts. In the ray-theoretical framework of Kirchhoff migration (or the generalized Radon transform) these effects can be straightforwardly computed and incorporated in a sensitivity-resolution analysis (see, for example, [20]). In this paper, we develop a technique that addresses these illumination effects in the framework of wave-equation migration. Throughout we assume the single scattering approximation for reflection seismic data.

We develop a comprehensive framework for target-oriented illumination analysis and introduce an illumination "correction" that simultaneously accounts for limited acquisition aperture and compensates for the so-called normal operator in inverse scattering to yield a "true-amplitude" image of reflectivity or local reflection coefficient, while minimizing distortions and artifacts. To carry out this analysis we make use of higher-dimensional "curvelets" and introduce associated matrix representations for the component operators, including the cutoffs or tapers determined by the acquisition aperture, that make up wave-equation migration.

The procedure we develop here contains elements of (regularized) Least-Squares migration ([26, 14]), double focusing (and the notion of controlled illumination, see [34, 1]), geophysical diffraction tomography ([21, 42]), and is motivated by the illumination analysis of [43] and [41]. Curvelets can be viewed as "fat", localized plane waves and hence form a natural candidate to generalize geophysical diffraction tomography, which relates the Fourier transform of reflection data to the Fourier transform of the image, valid in constant background media to heterogeneous background media. Indeed, we will develop a relation between curvelet coefficients representing the image and the curvelet coefficients representing the (downward continued) data. The coefficients also immediately provide information about the directional dependence, that is, downward continued wave slowness vectors and image dips, and implicitly scattering angle (and azimuth). Indeed, the curvelet transform reveals the imprint of the ray geometry underlying the wave-equation illumination analysis which can be used as part of an imaging condition.

There have been various approaches to carrying out illumination analysis using ray-based techniques: [31, 32], [30], [5] and [25] discuss the effects of a complex velocity model on illumination and spatial resolution through the introduction of a resolution function. [33] develops an illumination-

*Center for Computational and Applied Mathematics and Geo-Mathematical Imaging Group, Purdue University, West Lafayette, IN 47907, USA

†Center for Computational and Applied Mathematics and Geo-Mathematical Imaging Group, Purdue University, West Lafayette, IN 47907, USA

‡Department of Petroleum Engineering and Applied Geophysics, Norwegian University of Science and Technology, Trondheim, Norway

based normalization for wave-equation migration. [39] essentially constructs "a posteriori" pseudodifferential factors that correct (after migration) for illumination effects; this method requires the computation of the normal operator.

The frame of curvelets was introduced by [35]; digital curvelets and an associated discrete transform pair were developed by [9, 10, 11] and [8]. Curvelets were introduced in common-offset migration (to leading order) by [22]. [19] introduced imaging with the generalized Radon transform (GRT) and partial reconstruction using curvelets. Almost symmetric, discrete wave packets generating a higher-dimensional "curvelet" transform pair following [35] have been designed by [23]. The problem of compressing reflection data on the one hand and (extended) images of reflectors on the other hand, through *nonlinear* approximation by sums of wave packets, was addressed by [2]. Velocity differentiation and wave-equation tomography with wave packets were derived by [6]. Curvelets can also be used efficiently in residual migration ([12]) and general velocity continuation ([24]).

[3] derived and developed a multi-scale approach to wave propagation by solving a Volterra equation yielding the concentration of wave packets even in velocity models of limited smoothness. Building on this result, here, we develop the downward continuation counterpart of partial reconstruction based on the GRT ([19]). Our point of departure is the unifying formulation for seismic inverse scattering by [37, 38]. In our derivation we will point out analogies with the illumination analysis introduced by [29, 43, 41]. We go beyond the latter analysis by connecting the data illumination with the normal operator both for generating images as well as common-image-point gathers.

Curvelets are different from "beamlets" ([13]). Curvelets provide the harmonic analysis tool to sparsely represent the propagators ([35, 7]) and localize the normal operator. In particular, one can obtain the inverse of the normal operator matrix via diagonal approximation ([19]). The curvelet amplitude spectra are essentially window functions while curvelets themselves are well localized with decay tracing oriented ellipsoids. "Beamlets", on the other hand, are generated by windowed Fourier transforms.

The outline of the paper is as follows. In the next section, we begin with summarizing modelling of reflection seismic data in the Born approximation via extensions of the velocity contrast, and introduce the single scattering operator. The extensions yield a contrast function with the appearance of subsurface data. In the third section, we summarize directional (up/down) wavefield decomposition, introduce the double-square root (DSR) equation and discuss the associated thin-slab propagator. In the fourth section, we carry out the curvelet decomposition of the single scattering operator leading to its associated matrix representation, while separating out the wave diffraction within each thin slab. Using this decomposition, we derive the extended wave-equation imaging operator matrix adapted to contain an illumination correction, and then incorporate the compensation for the normal operator, within each thin slab, to arrive at the diffraction formulation of partial reconstruction. In the fifth section, we derive a formulation of partial reconstruction in terms of reflectivity and common-image-point gathers. A numerical illustration of the illumination correction, in terms of curvelets, common in both formulations is presented in the sixth section. We end with some conclusions.

We use the following Fourier-transform convention: ∂_t corresponds with $\mathrm{i}\omega$, that is, $D_t = \mathrm{i}^{-1}\partial_t$ corresponds with frequency ω while $D_x = \mathrm{i}^{-1}\partial_x$ corresponds with wavevector ξ_x.

2. Single scattering. We introduce an n-dimensional half space equipped with coordinates $(z, x) \in \mathbb{R}_+ \times \mathbb{R}^{n-1}$; z stands for depth ($n = 2, 3$). The earth's surface forms the top of the half space at $z = 0$. Source positions then have coordinates $(z = 0, s)$ and receiver positions have coordinates $(z = 0, r)$.

The causal acoustic Green's function $G(z, x, t, z', x')$ for a point source at (z', x') is the solution

of

$$\left[c(z,x)^{-2}\partial_t^2 - \partial_z^2 - \sum_{j=1}^{n-1} \partial_{x_j}^2 \right] G(z,x,t,z',x') = \delta(z-z')\delta(x-x')\delta(t), \tag{2.1}$$

with $G = 0, t < 0$. Migration is commonly based on the Born or single scattering approximation. Linearization of the wave equation yields for the corresponding perturbation of the Green's function,

$$\left[c_0(z,x)^{-2}\partial_t^2 - \partial_z^2 - \sum_{j=1}^{n-1} \partial_{x_j}^2 \right] \delta G(z,x,t,z',x') = 2\left(\frac{\delta c}{c_0^3}\right)(z,x)\,\frac{\partial^2 G}{\partial t^2}(z,x,t,z',x'). \tag{2.2}$$

Born approximation: A summary. Following [37], we write the Born approximation for single scattered waves in the form

$$\begin{aligned}\delta G(0,r,t,0,s) = \int_{\mathbb{R}^{n-1}\times\mathbb{R}_+}\int_{\mathbb{R}^{n-1}}\int_{-\infty}^{t}\int_{\mathbb{R}_+} & G(0,r,t-t_0,z,x) \\ & \times\, \partial_{t_0}^2 R(z,x,\bar{x},t_0-\bar{t}_0) G(z,\bar{x},\bar{t}_0,0,s)\,\mathrm{d}\bar{t}_0\,\mathrm{d}t_0\,\mathrm{d}\bar{x}\,\mathrm{d}x\mathrm{d}z,\end{aligned} \tag{2.3}$$

where

$$R(z,x,\bar{x},t_0) = \delta(t_0)\delta(x-\bar{x})2\left(\frac{\delta c}{c_0^3}\right)\left(z,\frac{\bar{x}+x}{2}\right), \tag{2.4}$$

or

$$R = E_2 E_1 2c_0^{-3}\delta c \tag{2.5}$$

with

$$E_1 :\ (c_0^{-3}\delta c)(z,x) \mapsto h(z,\bar{x},x) = \delta(x-\bar{x})2(c_0^{-3}\delta c)(z,\tfrac{\bar{x}+x}{2}), \tag{2.6}$$

$$E_2 :\ h(z,\bar{x},x) \mapsto R(z,x,\bar{x},t) = \delta(t)h(z,\bar{x},x). \tag{2.7}$$

Changing variables of integration, that is, $t_0 \mapsto t_0' = t_0 - \bar{t}_0$, (2.3) can be written in the form of an integral operator acting on the distribution R,

$$\begin{aligned}\delta G(0,r,t,0,s) = \int_{\mathbb{R}_+}\Bigg\{\int_{\mathbb{R}}\int_{\mathbb{R}^{n-1}}\int_{\mathbb{R}^{n-1}}\Bigg(\int_{\mathbb{R}_+} & G(0,r,t-t_0'-\bar{t}_0,z,x) \\ & \times\, G(z,\bar{x},\bar{t}_0,0,s)\,\mathrm{d}\bar{t}_0\Bigg)\partial_{t_0'}^2 R(z,x,\bar{x},t_0')\,\mathrm{d}\bar{x}\,\mathrm{d}x\,\mathrm{d}t_0'\Bigg\}\mathrm{d}z,\end{aligned} \tag{2.8}$$

in between the braces, the contributions of which are integrated over depth z.

Using the reciprocity relation of the time-convolution type for the Green's function, we obtain the integral representation

$$\begin{aligned}\delta G(0,r,t,0,s) = \int_{\mathbb{R}_+}\Bigg\{\int_{\mathbb{R}^{n-1}}\int_{\mathbb{R}^{n-1}}\int_{\mathbb{R}}\Bigg(\int_0^{t-t_0} & G(0,r,t-t_0-\bar{t}_0,z,x) \\ & \times\, G(0,s,\bar{t}_0,z,\bar{x})\,\mathrm{d}\bar{t}_0\Bigg)\partial_{t_0}^2 R(z,x,\bar{x},t_0)\,\mathrm{d}\bar{x}\,\mathrm{d}x\,\mathrm{d}t_0\Bigg\}\mathrm{d}z.\end{aligned} \tag{2.9}$$

Upon substituting (2.4) into this representation, we obtain a mapping $\delta c(z,x) \to \delta G(0,r,t,0,s)$ describing the single scattering of waves. The operator kernel (in between parentheses) appears to

propagate singularities from two different scattering points, $\bar{x}$ and x, at each depth z, to the surface at $z = 0$. We use the mapping

$$LR(s,r,t) = \int_{\mathbb{R}_+} \Big\{ \int_{\mathbb{R}^{n-1}} \int_{\mathbb{R}^{n-1}} \int_{\mathbb{R}} \Big(\int_0^{t-t_0} G(0,r,t-t_0-\bar{t}_0,z,x) \times G(0,s,\bar{t}_0,z,\bar{x})\,\mathrm{d}\bar{t}_0 \Big) R(z,x,\bar{x},t_0)\,\mathrm{d}\bar{x}\,\mathrm{d}x\,\mathrm{d}t_0 \Big\} \mathrm{d}z. \tag{2.10}$$

The scattering operator then follows to be

$$F:\ \delta c \mapsto LE_2E_1 2c_0^{-3}\delta c; \tag{2.11}$$

it models deconvolved seismic reflection data, where the deconvolution includes ∂_t^{-2}.

3. One-way wave propagation.

3.1. Directional decomposition: A summary. Directional (up/down) decomposition of transient waves – in the "flux normalization" (see, for example, [16]) – is accomplished through the introduction of pseudodifferential operator, $Q_-(z,.) = Q_-(z,x,D_x,D_t)$, with so-called principal symbol,

$$\mathrm{i}\ \mathrm{sgn}(\omega)|\omega|^{-1/2}[c_0(z,x)^{-2} - \omega^{-2}\|\xi_x\|^2]^{-1/4}.$$

A pseudodifferential operator is an integral operator. The (distribution) kernel, $((Q_-(z,.)))$, of $Q_-(z,.)$ relates to its symbol as

$$((Q_-(z,.)))(x,t,x',t') = (2\pi)^{-n} \int\int Q_-(z,x,\xi_x,\omega)\ \exp[\langle \xi_x, x-x'\rangle] \exp[\mathrm{i}\omega(t-t')]\,\mathrm{d}\xi_x \mathrm{d}\omega. \tag{3.1}$$

The one-way wave operator for upward propagation is written as

$$\partial_z - \mathrm{i}B_-(z,x,D_x,D_t) - C(z,x,D_x,D_t),$$

where $B_-(z,.)$ is the (negative) square-root operator with principal symbol given by

$$b(z,x,\xi_x,\omega) = \omega[c_0(z,x)^{-2} - \omega^{-2}\|\xi_x\|^2]^{1/2},$$

and $C(z,.)$ is a first-order, attenuative, pseudodifferential operator – suppressing "evanescent" constituents – with homogeneous, nonnegative real principal symbol, satisfying certain estimates ([36]). We will suppress the presence of this operator in our notation. To obtain a dynamically correct one-way wave equation, one needs to take the subprincipal symbol of $B_-(z,.)$ into account. We denote the upward propagator as $G_-(z,.)$.

Consider

$$u_-(z,.) = \int_z^\infty G_-(z,z_0) \left(\frac{1}{2}\mathcal{H}Q_-(z_0) \right) f(z_0,.)\,\mathrm{d}z_0, \tag{3.2}$$

where $\mathcal{H}$ denotes the Hilbert transform in time (with frequency representation $\mathrm{i}\,\mathrm{sgn}(\omega)$), assuming also that $f = 0$ on a neighborhood of the plane at depth z. Let $Q_-^*(z)$ denote the L^2 adjoint of $Q_-(z)$. We have that $Q_-^*(z)u_-(z,.) \equiv u(z,.)$, where u is the solution to the two-way wave equation,

$$\left[c_0(z,x)^{-2}\partial_t^2 - \partial_z^2 - \sum_{j=1}^{n-1} \partial_{x_j}^2 \right] u = f, \tag{3.3}$$

with f replaced by $(\psi_1(z_0,z) - Q_-^{-1}(z_0)[Q_-(z_0),\psi_1(z_0,z)])f$; ψ_1 is a taper to suppress singularities of the one-way solution which are incorrect in the sense that they do not correspond to solutions of the two-way wave equation. The square brackets denote a commutator. This establishes the relation between one-way wave propagation and the two-way wave equation.

3.2. Double-square-root (DSR) propagator. The double-square-root (DSR) propagator is given by

$$(H(z,z_0))(s,r,t,s_0,r_0,t_0) = \int_{\mathbb{R}} (G_-(z,z_0))(s,t-t_0-\bar{t}_0,s_0)(G_-(z,z_0))(r,\bar{t}_0,r_0)\,\mathrm{d}\bar{t}_0. \tag{3.4}$$

Here $(G_-(z,z_0))(r,\bar{t}_0,r_0,0)$ denotes the distribution kernel of $G_-(z,z_0)$, and $(H(z,z_0))(s,r,t,s_0,r_0,t_0)$ denotes the distribution kernel of $H(z,z_0)$ and is the Green's function of the DSR equation,

$$\left[\frac{\partial}{\partial z} - \mathrm{i}\Gamma(z,s,r,D_s,D_r,D_t)\right] u = 0, \tag{3.5}$$

$$\Gamma(z,s,r,D_s,D_r,D_t) = B_-(z,s,D_s,D_t) + B_-(z,r,D_r,D_t).$$

The propagation of singularities by this Green's function is described by (source and receiver) rays in phase space; the solution of the relevant Hamilton equations (by ray tracing) is denoted by $\Sigma_H(z,z_0)$.

The discussion following (3.2) implies that the upward continuation analogue of (2.10) is given by ([37])

$$LR := -\frac{1}{4} Q^*_{-,s}(0) Q^*_{-,r}(0) \int_{\mathbb{R}_+} H(0,z) Q_{-,s}(z) Q_{-,r}(z) R(z,.,.,.)\,\mathrm{d}z, \tag{3.6}$$

using that $\mathcal{H}^2 = -1$, and identifying $\bar{x}$ with the (subsurface) source (s) coordinates and x with the (subsurface) receiver (r) coordinates.

The DSR propagator can be approximated by a composition of thin-slab propagators ([17, 27]); one such thin-slab propagator attains the form

$$(H(z'-\Delta,z'))(s,r,t,s',r',t') \approx (2\pi)^{-(2n-1)} \iiint \exp[\mathrm{i}(\langle \xi_s, s-s'\rangle + \langle \xi_r, r-r'\rangle - \Delta\,\Gamma(z',s,r,\xi_s,\xi_r,\omega))] \exp[\mathrm{i}\omega(t-t')]\,\mathrm{d}\xi_s \mathrm{d}\xi_r \mathrm{d}\omega. \tag{3.7}$$

This approximation has an error roughly of order $\Delta^{1/2}$.

4. Diffraction formulation. Here, we develop a description of the single scattering operator (cf. (2.11)) in terms of "curvelets", which leads to the matrix representations for the component operators, $Q_-(.)$ and L (cf. (3.6)) while making use of (3.7).

4.1. Decomposition of the scattering operator into curvelets. Through composition (2.11), we build up the action of F on a curvelet. The frame of curvelets, $\{\varphi_\gamma\}$ (we use an index subscript zero if the curvelet is defined on contrast space, otherwise the curvelet is defined on (subsurface) data space) is introduced in Appendix A. We consider $2c_0^{-3}\delta c = \varphi_{\gamma_0}$, with $\gamma_0 = ((z_{j0},x_{j0}),\nu_0,k_0)$, which we can think of as being approximately supported on an oriented ellipsoid, centered at (z_{j0},x_{j0}) in space and $(\xi_z,\xi_x) = 2^{k_0}\nu_0$ in wavenumber; ν_0 can be thought of as a dip. The points (z_{j0},x_{j0}) lie on a tilted lattice; see Fig. 1. The extensions (cf. (2.6)-(2.7)) act on a curvelet as

$$\begin{aligned} E_2E_1\varphi_{\gamma_0}(z,s,r,t) &= (2\pi)^{-2n} \iiint\int \hat{\varphi}_{\nu_0,k_0}(\xi_z,\xi_s+\xi_r) \exp[\mathrm{i}\omega t] \exp[\mathrm{i}\xi_z(z-z_{j0})] \\ &\times \exp\left[\mathrm{i}\left\langle \xi_s+\xi_r, \frac{s+r}{2} - x_{j0}\right\rangle\right] \exp\left[-\mathrm{i}\left\langle \frac{\xi_s-\xi_r}{2}, r-s\right\rangle\right] \mathrm{d}\xi_s\mathrm{d}\xi_r\mathrm{d}\xi_z\mathrm{d}\omega \\ &= (2\pi)^{-2n} \iiint\int \hat{\varphi}_{\nu_0,k_0}(\xi_z,\xi_s+\xi_r) \exp[\mathrm{i}\omega t] \exp[\mathrm{i}\xi_z(z-z_{j0})] \\ &\times \exp[\mathrm{i}\langle \xi_s, s-x_{j0}\rangle] \exp[\mathrm{i}\langle \xi_r, r-x_{j0}\rangle]\,\mathrm{d}\xi_z\mathrm{d}\xi_s\mathrm{d}\xi_r\mathrm{d}\omega. \end{aligned} \tag{4.1}$$

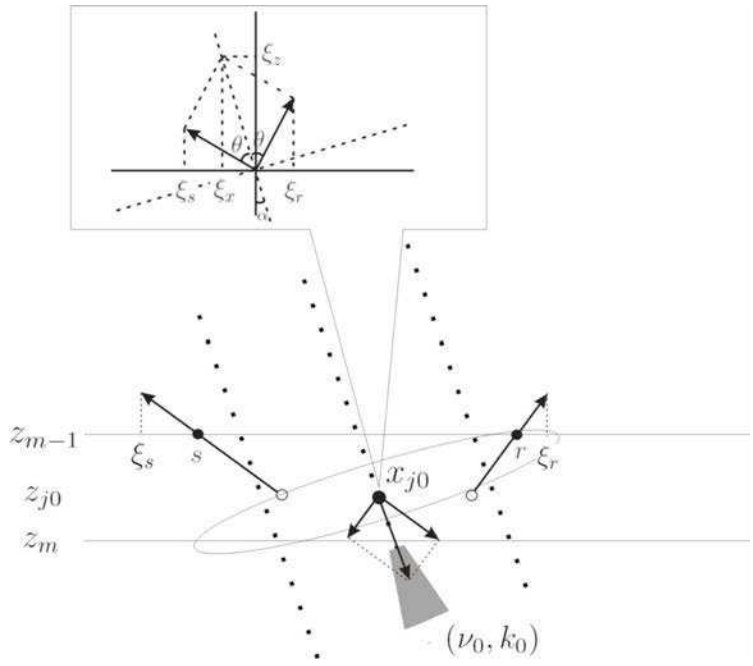

FIG. 1. *Coupling microdiffraction to illumination analysis: Dipping contrast curvelet (indicated by the ellipse), source and receiver wave vectors, lattice of translations and thin slab.*

Applying the composition of operators, $Q_{-,s}(z)Q_{-,r}(z)$, yields

$$(4.2)\quad Q_{-,s}(z)Q_{-,r}(z)E_2E_1\varphi_{\gamma_0}(z,s,r,t) = (2\pi)^{-2n}\int\!\!\int\!\!\int\!\!\int Q_{-,s}(z,s,\xi_s,\omega)Q_{-,r}(z,r,\xi_r,\omega) \times \hat{\varphi}_{\nu_0,k_0}(\xi_z,\xi_s+\xi_r)\exp[\mathrm{i}\omega t]\exp[\mathrm{i}\xi_z(z-z_{j0})] \times \exp[\mathrm{i}\langle\xi_s,s-x_{j0}\rangle]\exp[\mathrm{i}\langle\xi_r,r-x_{j0}\rangle]\,\mathrm{d}\xi_z\mathrm{d}\xi_s\mathrm{d}\xi_r\mathrm{d}\omega.$$

We decompose the integration in depth in L into thin slab integrations (based on the so-called Trotter product, while assuming that $z_m - z_{m-1} = \Delta$ is sufficiently small, see [18]), that is,

$$(4.3)\quad LR = -\frac{1}{4}Q^*_{-,s}(0)Q^*_{-,r}(0)\sum_{m=1}^{\infty} H(0,z_{m-1})V(z_{m-1},.,.,.) \quad \text{with}$$
$$V(z_{m-1},.,.,.) = \int_{z_{m-1}}^{z_m} H(z_{m-1},z)Q_{-,s}(z)Q_{-,r}(z)R(z,.,.,.)\,\mathrm{d}z, \quad z_0 = 0,$$

cf. (3.6), and isolate the contribution from the slab $[z_{m-1}, z_m)$ that contains z_{j0}. We substitute (4.2) and expression (3.7) for the thin-slab propagator, and obtain

$$(4.4)\quad V_{\gamma_0}(z_{m-1},s,r,t) = \int_{z_{m-1}}^{z_m} H(z_{m-1},z)Q_{-,s}(z)Q_{-,r}(z)E_2E_1\varphi_{\gamma_0}(z,.,.,.)\,\mathrm{d}z \approx \int_{z_{m-1}}^{z_m}$$
$$(2\pi)^{-2n}\int\!\!\int\!\!\int\!\!\int \exp[\mathrm{i}(\langle\xi_s,s-x_{j0}\rangle + \langle\xi_r,r-x_{j0}\rangle - (z-z_{m-1})\,\Gamma(z_m,s,r,\xi_s,\xi_r,\omega))] \times \exp[\mathrm{i}\omega t]Q_{-,s}(z,s,\xi_s,\omega)Q_{-,r}(z,r,\xi_r,\omega) \times \hat{\varphi}_{\nu_0,k_0}(\xi_z,\xi_s+\xi_r)\exp[\mathrm{i}\xi_z(z-z_{j0})]\,\mathrm{d}\xi_s\mathrm{d}\xi_r\mathrm{d}\omega\;\mathrm{d}\xi_z\mathrm{d}z.$$

We apply the method of stationary phase,

$$(4.5)\quad (2\pi)^{-1}\int_{z_{m-1}}^{z_m}\int Q_{-,s}(z,s,\xi_s,\omega)Q_{-,r}(z,r,\xi_r,\omega)\hat{\varphi}_{\nu_0,k_0}(\xi_z,\xi_s+\xi_r)$$
$$\times\ \exp[-\mathrm{i}(z-z_{m-1})\,\Gamma(z_m,s,r,\xi_s,\xi_r,\omega)]\exp[\mathrm{i}\xi_z(z-z_{j0})]\,\mathrm{d}\xi_z\mathrm{d}z$$
$$\approx Q_{-,s}(z_{j0},s,\xi_s,\omega)Q_{-,s}(z_{j0},r,\xi_r,\omega)\,\hat{\varphi}_{\nu_0,k_0}(\Gamma(z_m,s,r,\xi_s,\xi_r,\omega),\xi_s+\xi_r)$$
$$\times\ \exp[-\mathrm{i}(z_{j0}-z_{m-1})\,\Gamma(z_m,s,r,\xi_s,\xi_r,\omega)],$$

using that the stationary point is given by $z=z_{j0}$, $\xi_z=\Gamma(z_m,s,r,\xi_s,\xi_r,\omega)$, so that

$$(4.6)\quad V_{\gamma_0}(z_{m-1},s,r,t)\approx(2\pi)^{-(2n-1)}\int\int\int Q_{-,s}(z_{j0},s,\xi_s,\omega)Q_{-,r}(z_{j0},r,\xi_r,\omega)$$
$$\times\ \hat{\varphi}_{\nu_0,k_0}(\Gamma(z_m,s,r,\xi_s,\xi_r,\omega),\xi_s+\xi_r)\,\exp[-\mathrm{i}(z_{j0}-z_{m-1})\,\Gamma(z_m,s,r,\xi_s,\xi_r,\omega)]$$
$$\times\ \exp[\mathrm{i}(\langle\xi_s,s-x_{j0}\rangle+\langle\xi_r,r-x_{j0}\rangle+\omega t)]\,\mathrm{d}\xi_s\mathrm{d}\xi_r\mathrm{d}\omega,$$

which is viewed as a mapping of the contrast curvelet, φ_{γ_0}, to virtual subsurface reflection data, $V_{\gamma_0}(z_{m-1},.,.,.)$, provided that $z_{j0}\in(z_{m-1},z_m)$ – we assume that the z_{j0} do not coincide with z_m, $m=0,1,2,\ldots$; see Fig. 1. We expand $V_{\gamma_0}(z_{m-1},.,.,.)$ into curvelets, that is,

$$V_{\gamma_0}(z_{m-1},.,.,.)=\sum_{\gamma'}V_{\gamma';\gamma_0}(z_{m-1})\varphi_{\gamma'},\qquad V_{\gamma';\gamma_0}(z_{m-1}):=\langle\psi_{\gamma'},V_{\gamma_0}(z_{m-1},.,.,.)\rangle_{(s,r,t)};$$

the inner products are readily evaluated in the Fourier domain with (4.6). We will encounter two alternative versions of these elements while developing strategies for partial reconstruction.

The matrix for the (invertible) propagator $H(0,z_{m-1})$ is denoted by $[H(0,z_{m-1})]$. Furthermore, let $[Q^*_{-,s}(0)Q^*_{-,r}(0)]$ denote the matrix associated with pseudodifferential operator $Q^*_{-,s}(0)Q^*_{-,r}(0)$. Both matrices are sparse ([19]). We find that the matrix elements of F attain the form

$$(4.7)\qquad \langle\psi_\gamma,F\varphi_{\gamma_0}\rangle_{(s,r,t)}=-\frac{1}{4}\sum_{\gamma''}[Q^*_{-,s}(0)Q^*_{-,r}(0)]_{\gamma\gamma''}\sum_{m=1}^{\infty}\sum_{\gamma'}\,[H(0,z_{m-1})]_{\gamma''\gamma'}V_{\gamma';\gamma_0}(z_{m-1}).$$

For given γ_0, one term, m_0 say, dominates the summation: For given Δ and sufficiently fine scale, k_0, the curvelet is almost localized (cf. (A.3)) to the thin slab $[z_{m_0-1},z_{m_0})\ni z_{j0}$.

4.2. Migration and micro-diffraction tomography. Here, we describe imaging in the downward continuation approach in terms of "curvelets". We decompose the surface reflection data, $d=\sum_\gamma d_\gamma\psi_\gamma$; we write (d) for the sequence of coefficients d_γ. We let the adjoint, F^*, of F, act on a data curvelet, ψ_γ,

$$(4.8)\quad F^*\psi_\gamma(z,.)=R_1R_2Q^*_{-,s}(z)Q^*_{-,r}(z)$$
$$\sum_{\bar\gamma',\bar\gamma''}H(z_{\bar m-1},z)^*\psi_{\bar\gamma'}\ [H(0,z_{\bar m-1})^*]_{\bar\gamma'\bar\gamma''}[Q_{-,s}(0)Q_{-,r}(0)]_{\bar\gamma''\gamma}\left(-\frac{1}{4}\right),$$

if $z\in[z_{\bar m-1},z_{\bar m})$; here, $R_1=E_1^*$ and $R_2=E_2^*$ are restrictions representing the traditional imaging conditions setting time (R_2) and subsurface offset (R_1) to zero. If curvelet components, d_γ, with index γ in the set $\mathcal{S}$ can be observed at the surface ($\mathcal{S}$ is derived from the acquisition geometry), the associated subsurface illumination is captured in the matrix

$$(4.9)\quad [A^{\mathcal{S}}(z_{\bar m-1},z_{m-1})]_{\bar\gamma'\gamma'}=\sum_{\bar\gamma'',\gamma,\tilde\gamma,\gamma''}[H(0,z_{\bar m-1})^*]_{\bar\gamma'\bar\gamma''}[Q_{-,s}(0)Q_{-,r}(0)]_{\bar\gamma''\gamma}$$
$$\times\ \Pi^{\mathcal{S}}_{\gamma\tilde\gamma}\ [Q^*_{-,s}(0)Q^*_{-,r}(0)]_{\tilde\gamma\gamma''}[H(0,z_{m-1})]_{\gamma''\gamma'}$$

with $\Pi^{\mathcal{S}} = \Pi\ \mathbf{1}^{\mathcal{S}}$, which can be loosely thought of as a projection onto $\mathcal{S}$; for the introduction of Π, see Appendix A. The inverse diagonal approximation of $[A^{\mathcal{S}}(z_{m-1}, z_{m-1})]$ is given by

$$\widetilde{D}_{\gamma'}(z_{m-1})^{-1} = [A^{\mathcal{S}}(z_{m-1}, z_{m-1})]^{-1}_{\gamma'\gamma'}\Pi_{\gamma'\gamma'};$$

this approximation reflects the inverse of $[A^{\mathcal{S}}(z_{m-1}, z_{m-1})]$ up to an error of order $2^{-k/2}$ ([19]). We introduce the illumination-corrected imaging operator via the images of data curvelets, ψ_γ,

$$(F^*)'\psi_\gamma(z,.) = R_1R_2Q^*_{-,s}(z)Q^*_{-,r}(z) \sum_{\bar\gamma',\bar\gamma''} H(z_{\bar m-1}, z)^*\psi_{\bar\gamma'}\ \widetilde{D}_{\bar\gamma'}(z_{\bar m-1})^{-1}[H(0, z_{\bar m-1})^*]_{\bar\gamma'\bar\gamma''}[Q_{-,s}(0)Q_{-,r}(0)]_{\bar\gamma''\gamma}\left(-\frac{1}{4}\right), \tag{4.10}$$

if $z \in [z_{\bar m-1}, z_{\bar m})$. We write

$$V^*_{\bar\gamma'}(z_{\bar m-1}, z, .) := R_1R_2Q^*_{-,s}(z)Q^*_{-,r}(z)H(z_{\bar m-1}, z)^*\psi_{\bar\gamma'}$$

for the image in slab $\bar m$ using the illumination-corrected downward continued curvelet, $\psi_{\bar\gamma'}$, as data. Then

$$\langle (F^*)'\psi_\gamma, \varphi_{\bar\gamma_0}\rangle_{(z,x)} = \sum_{\bar m=1}^{\infty}\sum_{\bar\gamma',\bar\gamma''} V^*_{\bar\gamma_0;\bar\gamma'}(z_{\bar m-1}) \times \overline{\widetilde{D}_{\bar\gamma'}(z_{\bar m-1})^{-1}[H(0, z_{\bar m-1})^*]_{\bar\gamma'\bar\gamma''}[Q_{-,s}(0)Q_{-,r}(0)]_{\bar\gamma''\gamma}}\left(-\frac{1}{4}\right), \tag{4.11}$$

where

$$V^*_{\bar\gamma_0;\bar\gamma'}(z_{\bar m-1}) = \int_{z_{\bar m-1}}^{z_{\bar m}}\int \overline{V^*_{\bar\gamma'}(z_{\bar m-1}, z, .)}\,\varphi_{\bar\gamma_0}(z,.)\,\mathrm{d}x\mathrm{d}z = V_{\bar\gamma';\bar\gamma_0}(z_{\bar m-1}). \tag{4.12}$$

For given $\bar\gamma_0$, one term, $\bar m_0$, dominates the summation: For given Δ and sufficiently fine scale, $\bar k_0$, the curvelet is almost localized (cf. (A.3)) to the thin slab $[z_{\bar m_0-1}, z_{\bar m_0}) \ni z_{\bar\jmath 0}$.

Using the thin-slab propagator, $V^*_{\bar\gamma'}(z_{\bar m-1}, ., .)$ can be expressed in terms of a mapping of the virtual subsurface data curvelet, $\psi_{\bar\gamma'}$, to an image reflecting the restrictions,

$$\begin{aligned} V^*_{\bar\gamma'}(z_{\bar m-1}, z, x) \approx (2\pi)^{-(2n-1)} \int\!\!\int\!\!\int\ \int\!\!\int\!\!\int \\ \left|\frac{\partial \mathit{\Gamma}}{\partial\omega}(z_{\bar m}, s, r, \tfrac{1}{2}\xi_x - \theta, \tfrac{1}{2}\xi_x + \theta, \mathit{\Gamma}^{-1}(z_{\bar m}, s, r, \xi_z, \tfrac{1}{2}\xi_x - \theta, \tfrac{1}{2}\xi_x + \theta))\right|^{-1} \\ \times\ \overline{Q_{-,s}(z, s, \tfrac{1}{2}\xi_x - \theta, \mathit{\Gamma}^{-1}(z_{\bar m}, s, r, \xi_z, \tfrac{1}{2}\xi_x - \theta, \tfrac{1}{2}\xi_x + \theta))} \\ \times\ \overline{Q_{-,r}(z, r, \tfrac{1}{2}\xi_x + \theta, \mathit{\Gamma}^{-1}(z_{\bar m}, s, r, \xi_z, \tfrac{1}{2}\xi_x - \theta, \tfrac{1}{2}\xi_x + \theta))} \\ \times\ \psi_{\bar\gamma'}(s, r, t)\ \exp[-\mathrm{i}\,\mathit{\Gamma}^{-1}(z_{\bar m}, s, r, \xi_z, \tfrac{1}{2}\xi_x - \theta, \tfrac{1}{2}\xi_x + \theta)\,t] \\ \times\ \exp\left[\mathrm{i}\left(\left\langle \xi_x, x - \frac{s+r}{2}\right\rangle - \langle\theta, r - s\rangle + \xi_z(z - z_{\bar m-1})\right)\right]\mathrm{d}s\mathrm{d}r\mathrm{d}t\,\mathrm{d}\theta\ \mathrm{d}\xi_z\mathrm{d}\xi_x, \end{aligned} \tag{4.13}$$

upon invoking a change of variables of integration, following the invertible mapping, $\omega \mapsto \xi_z = \mathit{\Gamma}$ ([37, Lemma 4.1]) and subsequently setting $\xi_s = \frac{1}{2}\xi_x - \theta$, $\xi_r = \frac{1}{2}\xi_x + \theta$. We recognize a Stolt-like migration. We note that θ is related to scattering angle and azimuth associated with the underlying ray geometry, see [17]; ξ_x and θ as well as ξ_z are constrained by the support of $\hat\psi_{\bar\nu',\bar k'}$.

4.3. Reconstruction. Here, we analyze the relationship between the illumination-corrected image and the contrast. We arrive at a normal operator for "micro"-diffraction tomography: The illumination-corrected image corresponds with $\widetilde{N}'\, 2c_0^{-3}\delta c$. Here, $\widetilde{N}' = (F^*)'\mathrm{C}^{-1}\Pi^{\mathcal{S}}\mathrm{C}F$, where C denotes the curvelet transform, with matrix representation

$$[\widetilde{N}']_{\bar\gamma_0\gamma_0} = \left(-\frac{1}{4}\right)^2 \sum_{\bar m,m=1}^{\infty} \sum_{\bar\gamma',\gamma'} V^*_{\bar\gamma_0;\bar\gamma'}(z_{\bar m-1})\widetilde{D}_{\bar\gamma'}(z_{\bar m-1})^{-1}[A^{\mathcal{S}}(z_{\bar m-1},z_{m-1})]_{\bar\gamma'\gamma'}V_{\gamma';\gamma_0}(z_{m-1}). \tag{4.14}$$

Because $\widetilde{N}'$ is a pseudodifferential operator, its corresponding matrix $[\widetilde{N}']$ is diagonally dominant, while

$$[\widetilde{N}']_{\gamma_0\gamma_0} \approx \left(-\frac{1}{4}\right)^2 \sum_{\bar\gamma',\gamma'} V^*_{\gamma_0;\bar\gamma'}(z_{m_0-1})\widetilde{D}_{\bar\gamma'}(z_{m_0-1})^{-1}[A^{\mathcal{S}}(z_{m_0-1},z_{m_0-1})]_{\bar\gamma'\gamma'}V_{\gamma';\gamma_0}(z_{m_0-1}) \tag{4.15}$$

with $[z_{m_0-1}, z_{m_0}) \ni z_{j0}$ as before.

We set up the normal equations for the extended contrast, h (cf. (2.6)), which we subject to the decomposition, $h = \sum_{\gamma_0} h_{\gamma_0}\varphi_{\gamma_0}$. Thus, we redefine (cf. (4.4))

$$V_{\gamma';\gamma_0}(z_{m_0-1}) := [K_{m_0-1}]_{\gamma'\gamma_0}, \tag{4.16}$$

with

$$K_{m-1} \;:\; h \to \int_{z_{m-1}}^{z_m} H(z_{m-1},z')Q_{-,s}(z')Q_{-,r}(z')E_2h(z',.,.)\,\mathrm{d}z',$$

the propagation of singularities of which is described by a transformation, $\Sigma_{K;m-1}$ say, obtained by ray tracing.

We solve the normal equations in two steps. First, we consider subsurface data coefficients, $d_{\gamma'}(z_{m_0-1})$, replacing $\sum_{\tilde\gamma'}\Pi^{\mathcal{S}(z_{m_0-1})}_{\gamma'\tilde\gamma'}V_{\tilde\gamma';\gamma_0}(z_{m_0-1})$, if $\mathcal{S}(z_{m-1}) \subset \Sigma_H^{-1}(0,z_{m-1})(\mathcal{S})$. We carry out a "partial" redatuming by solving

$$\begin{aligned}\sum_{\gamma'} \widetilde{D}_{\bar\gamma'}(z_{m_0-1})^{-1}[A^{\mathcal{S}}(z_{m_0-1},z_{m_0-1})]_{\bar\gamma'\gamma'}d_{\gamma'}(z_{m_0-1}) \\ = \sum_{\bar\gamma'',\gamma,\tilde\gamma} \widetilde{D}_{\bar\gamma'}(z_{m_0-1})^{-1}[H(0,z_{m_0-1})^*]_{\bar\gamma'\bar\gamma''}[Q_{-,s}(0)Q_{-,r}(0)]_{\bar\gamma''\gamma}\left(-\frac{1}{4}\right)\Pi^{\mathcal{S}}_{\gamma\tilde\gamma}d_{\tilde\gamma},\end{aligned} \tag{4.17}$$

for (D). In Appendix A, we introduce the "distance" between indices, $\overline{d}$. We assume that $\overline{d}(\gamma,\Sigma_H(0,z_{m-1})(\gamma')) \ll 2^{-k}$ for $\gamma \in \mathcal{S}^c$ (^{c} denoting the complement) and $\gamma' \in \mathcal{S}(z_{m-1})$ at scale k. The retrofocusing of waves is now reflected by the property ([19])

$$\widetilde{D}(z_{m-1})^{-1}[A^{\mathcal{S}}(z_{m-1},z_{m-1})]\Pi^{\mathcal{S}(z_{m-1})} \approx \Pi^{\mathcal{S}(z_{m-1})}.$$

The second step concerns a micro-diffraction problem, in analogy with the notion of geophysical diffraction tomography. Following (4.15), we consider

$$\sum_{\bar\gamma',\gamma'} V^*_{\gamma_0;\bar\gamma'}(z_{m_0-1})\Pi^{\mathcal{S}(z_{m_0-1})}_{\bar\gamma'\gamma'}V_{\gamma';\gamma_0}(z_{m_0-1}) = ([K^*_{m_0-1}]\Pi^{\mathcal{S}(z_{m_0-1})}[K_{m_0-1}])_{\gamma_0\gamma_0}.$$

Let $\mathcal{C}(z_{m-1}) \subset \Sigma^{-1}_{K,m-1}(\mathcal{S}(z_{m-1}))$, assuming that $\overline{d}(\gamma,\Sigma_{K,m-1}(\gamma_1)) \ll 2^{-k}$ for $\gamma \in \mathcal{S}(z_{m-1})^c$ and $\gamma_1 \in \mathcal{C}(z_{m-1})$ at scale k. We then use the approximation,

$$K^*_{m-1}\mathrm{C}^{-1}\Pi^{\mathcal{S}(z_{m-1})}\mathrm{C}K_{m-1}\mathrm{C}^{-1}\Pi^{\mathcal{C}(z_{m-1})} \approx \Xi_{m-1}\mathrm{C}^{-1}\Pi^{\mathcal{C}(z_{m-1})}, \quad \text{with } \Xi_{m-1} = K^*_{m-1}K_{m-1}. \tag{4.18}$$

We note that the illumination is accounted for by the matrices $\Pi^{\mathcal{C}}$. The principal symbol of Ξ_{m-1}, the value of which is not explicitly dependent on m, follows to be ([38, Lemma 2.1])

$$\begin{aligned}(4.19)\quad &\Xi_{m-1}(z,s,r,\xi_z,\xi_s,\xi_r)\\ &= a_z(s,r,\xi_s,\xi_r,\Gamma^{-1}(z,s,r,\xi_z,\xi_s,\xi_r))\left|\frac{\partial\Gamma}{\partial\omega}(z,s,r,\xi_s,\xi_r,\Gamma^{-1}(z,s,r,\xi_z,\xi_s,\xi_r))\right|^{-1},\\ &\qquad\text{with}\quad a_z(s,r,\xi_s,\xi_r,\omega)=|b(z,s,\xi_s,\omega)|^{-1}|b(z,r,\xi_r,\omega)|^{-1},\quad z\in[z_{m-1},z_m);\end{aligned}$$

because Ξ_{m-1} is a pseudodifferential operator, its matrix representation, $[\Xi_{m-1}]$, is concentrated on the diagonal. If we substitute the thin-slab propagators as before,
$\Gamma^{-1}(z,s,r,\xi_z,\xi_s,\xi_r)$ in $\Xi_{m-1}(z,s,r,\xi_z,\xi_s,\xi_r)$ gets replaced by $\Gamma^{-1}(z_m,s,r,\xi_z,\xi_s,\xi_r)$. The inverse diagonal approximation of $[\Xi_{m-1}]$ is given by

$$(\widetilde{D}_{\Xi})_{\gamma_0}(z_{m-1})^{-1}=[\Xi_{m-1}]^{-1}_{\gamma_0\gamma_0}\Pi_{\gamma_0\gamma_0}.$$

We carry out the "partial" reconstruction by solving

$$\begin{aligned}(4.20)\quad &\widetilde{D}_{\Xi}(z_{m_0-1})^{-1}[K^*_{m_0-1}]\Pi^{\mathcal{S}(z_{m_0-1})}[K_{m_0-1}]\Pi^{\mathcal{C}(z_{m_0-1})}(h)\\ &\qquad=\widetilde{D}_{\Xi}(z_{m_0-1})^{-1}[K^*_{m_0-1}]\Pi^{\mathcal{S}(z_{m_0-1})}(d(z_{m_0-1}))\end{aligned}$$

for (h) upon substituting for $(d(z_{m_0-1}))$ the solution of (4.17), where

$$\widetilde{D}_{\Xi}(z_{m-1})^{-1}[K^*_{m-1}]\Pi^{\mathcal{S}(z_{m-1})}[K_{m-1}]\Pi^{\mathcal{C}(z_{m-1})}\approx\widetilde{D}_{\Xi}(z_{m-1})^{-1}[\Xi_{m-1}]\Pi^{\mathcal{C}(z_{m-1})}\approx\Pi^{\mathcal{C}(z_{m-1})}.$$

Remark. We briefly compare our results with the seismic illumination analysis of [43]: We make the following identifications

- the wavenumber domain "local reflectivity" (cf. (3))

$$\begin{aligned}m(\mathbf{r},\mathbf{k}_g+\mathbf{k}_s)\leftrightarrow\hat{\varphi}_{\nu_0,k_0}(&\Gamma(z_m,x,x,\xi_s,\xi_r,\omega),\xi_s+\xi_r)\\ &\exp[-\mathrm{i}\langle\xi_s+\xi_r,x_{j0}\rangle]\,\exp[-\mathrm{i}z_{j0}\Gamma(z_m,x,x,\xi_s,\xi_r,\omega)];\end{aligned}$$

- the local illumination matrix (cf. (10))

$$A(\mathbf{r},\mathbf{K}_s,\mathbf{K}_g)\leftrightarrow[A^{\mathcal{S}}(z_{m-1},z_{m-1})]_{\gamma'\gamma'}$$

  when viewed (on the diagonal) as a function of $2^{k'}\nu'$ in (ξ_s,ξ_r,ω)-space, for fixed $(s,r,t)_{j'}=(x_{j0},x_{j0},0)$;
- the wave vectors, $\mathbf{K}_r\leftrightarrow\theta$, $\mathbf{K}_d\leftrightarrow\xi_x$ (cf. (12));
- the dip, $\mathbf{n}\leftrightarrow\nu_0$;
- in the acquisition dip response (ADR): the role of $\delta(\mathbf{K}_g+\mathbf{K}_s-C\mathbf{N})$ in (13) is replaced by $V_{\gamma';\gamma_0}$; $D(\mathbf{r},\mathbf{n})\leftrightarrow[\widetilde{N}]_{\gamma_0\gamma_0}$ (diagonal factor $\widetilde{D}_{\bar{\gamma}'}(z_{\bar{m}-1})^{-1}$ omitted) assuming that $\mathbf{r}$ coincides with (z_{j0},x_{j0}), for any value of k_0.

5. Reflectivity and image-gathers formulation. Here, we reformulate the illumination analysis developed in the previous section in terms of (multi-scale) curvelet decompositions of common image-point gathers and reflectivity. The notion of reflectivity is tied to a surface-integral formulation for the scattering of waves.

5.1. Reflectivity and Kirchhoff approximation. Motivated by [15], [38] introduce the mapping, $r(z,x,p)\mapsto R(z,x,\bar{x},t)$, with

$$\begin{aligned}(5.1)\quad R(z,x,\bar{x},t)=(2\pi)^{-n}\int_{\mathbb{R}}\int_{\mathbb{R}^{n-1}}&r\left(z,\frac{\bar{x}+x}{2},p\right)\\ &\times\exp[\mathrm{i}\langle(\bar{x}-x),p\rangle\,\omega]\exp(\mathrm{i}\omega t)\,|\omega|^{n-1}\mathrm{d}p\mathrm{d}\omega,\end{aligned}$$

which we can write as an operator composition, $R = \Lambda E_3 r$, where Λ is a pseudodifferential operator with symbol $|\omega|^{n-1}$, and

$$E_3 r(z,\bar{x},x,t) = (2\pi)^{-(n-1)} \int_{\mathbb{R}^{n-1}} \delta(t - \langle (x-\bar{x}), p\rangle)\; r\left(z, \frac{\bar{x}+x}{2}, p\right)\, \mathrm{d}p. \tag{5.2}$$

The contrast formulation is recovered by setting

$$r = E_4(2c_0^{-3}\delta c),$$

where

$$E_4(2c_0^{-3}\delta c)(z,x,p) = (2c_0^{-3}\delta c)(z,x). \tag{5.3}$$

The quantity r describes the reflectivity. Indeed, the principal part of r can be associated with the plane-wave reflection coefficient. We introduce the operator,

$$\bar{F}:\; r \mapsto L\Lambda E_3 r.$$

As an example, we consider a horizontal reflector, Σ, at $z = z_\Sigma$. We can rewrite (2.3)-(2.4) in the form of a Kirchhoff approximation by replacing $\partial_{t_0}^2 R(z,x,\bar{x},t_0-\bar{t}_0)$ with $\partial_{t_0} R_1(z,x,\bar{x},t_0-\bar{t}_0)\delta(z-z_\Sigma)$, in which

$$R_1\delta(.-z_\Sigma) = E_2 E_1 2c_0^{-3} c', \quad c' = \partial_z \delta c,$$

yielding a surface integral over Σ. We can extend this representation by incorporating the linearized reflection coefficient,

$$r_1(z,x,p) = \frac{1}{2\left(1 - \dfrac{c_0^2\|p\|^2}{4}\right)} \frac{\epsilon}{c_0}\; 2[c_0^{-2} - \|p\|^2]^{1/2},$$

with $R_1 = \Lambda E_3 r_1$, if ϵ represents the jump in wavespeed, see [4].

5.2. Decomposition of the scattering operator into curvelets. Concerning the scattering operator, we only need to revisit the introduction of elements $V_{\gamma';\gamma_0}$. We consider $r = \varphi_{\gamma_0}$ – and view the projections onto the (z,x)-plane and the (z,p)-plane to reveal the localization in dip and scattering angle and azimuth.

With (5.1), we get

$$\begin{aligned}\Lambda E_3 \varphi_{\gamma_0}(z,s,r,t) = (2\pi)^{-3n+1} \int\int\int\int\int \hat{\varphi}_{\nu_0,k_0}(\xi_z,\xi_x,\xi_p) \\ \times\; \exp[-\mathrm{i}\langle (r-s),p\rangle\,\omega] \exp[\mathrm{i}\omega t]\, |\omega|^{n-1} \mathrm{d}p \mathrm{d}\omega \\ \times\; \exp[\mathrm{i}\xi_z(z-z_{j0})] \exp\left[\mathrm{i}\langle \xi_x, \frac{s+r}{2} - x_{j0}\rangle\right] \exp[\mathrm{i}\langle \xi_p, p-p_{j0}\rangle] \mathrm{d}\xi_z \mathrm{d}\xi_x \mathrm{d}\xi_p;\end{aligned}$$

Changing variables of integration, $\xi_x = \xi_s + \xi_r$ and $\omega p = \frac{1}{2}(\xi_s - \xi_r)$, leads to

$$\begin{aligned}\Lambda E_3 \varphi_{\gamma_0}(z,s,r,t) = (2\pi)^{-3n+1} \int\int\int\int\int \hat{\varphi}_{\nu_0,k_0}(\xi_z,\xi_s+\xi_r,\xi_p) \\ \times\; \exp\left[\mathrm{i}\langle \omega^{-1}\xi_p, \frac{\xi_s-\xi_r}{2} - \omega p_{j0}\rangle\right] \mathrm{d}\xi_p\; \exp[\mathrm{i}\xi_z(z-z_{j0})] \\ \times\; \exp[\mathrm{i}\langle \xi_s, s-x_{j0}\rangle] \exp[\mathrm{i}\langle \xi_r, r-x_{j0}\rangle] \exp[\mathrm{i}\omega t]\, \mathrm{d}\xi_z \mathrm{d}\xi_s \mathrm{d}\xi_r \mathrm{d}\omega.\end{aligned} \tag{5.4}$$

As before, $\frac{\xi_s-\xi_r}{2}=\omega p_{j0}$ can be associated with a scattering angle and azimuth. In analogy with (4.4), we have

$$V_{\gamma_0}(z_{m-1},s,r,t)=\int_{z_{m-1}}^{z_m}H(z_{m-1},z)Q_{-,s}(z)Q_{-,r}(z)\Lambda E_3\varphi_{\gamma_0}(z,.,.,.)\,\mathrm{d}z\approx\int_{z_{m-1}}^{z_m}\tag{5.5}$$
$$(2\pi)^{-3n+1}\int\int\int\int\int\exp[\mathrm{i}(\langle\xi_s,s-x_{j0}\rangle+\langle\xi_r,r-x_{j0}\rangle-(z-z_{m-1})\,\Gamma(z_m,s,r,\xi_s,\xi_r,\omega))]$$
$$\times\exp[\mathrm{i}\omega t]Q_{-,s}(z,s,\xi_s,\omega)Q_{-,r}(z,r,\xi_r,\omega)$$
$$\times\hat{\varphi}_{\nu_0,k_0}(\xi_z,\xi_s+\xi_r,\xi_p)\exp\left[\mathrm{i}\langle\omega^{-1}\xi_p,\frac{\xi_s-\xi_r}{2}-\omega p_{j0}\rangle\right]\mathrm{d}\xi_p\ \exp[\mathrm{i}\xi_z(z-z_{j0})]\,\mathrm{d}\xi_s\mathrm{d}\xi_r\mathrm{d}\omega\ \mathrm{d}\xi_z\mathrm{d}z.$$

We apply the method of stationary phase as before, and obtain

$$V_{\gamma_0}(z_{m-1},s,r,t)\approx(2\pi)^{-(3n-2)}\int\int\int Q_{-,s}(z_{j0},s,\xi_s,\omega)Q_{-,r}(z_{j0},r,\xi_r,\omega)\tag{5.6}$$
$$\int\hat{\varphi}_{\nu_0,k_0}(\Gamma(z_m,s,r,\xi_s,\xi_r,\omega),\xi_s+\xi_r,\xi_p)\exp\left[\mathrm{i}\langle\omega^{-1}\xi_p,\frac{\xi_s-\xi_r}{2}-\omega p_{j0}\rangle\right]\mathrm{d}\xi_p$$
$$\times\exp[-\mathrm{i}(z_{j0}-z_{m-1})\,\Gamma(z_m,s,r,\xi_s,\xi_r,\omega)]$$
$$\times\exp[\mathrm{i}(\langle\xi_s,s-x_{j0}\rangle+\langle\xi_r,r-x_{j0}\rangle+\omega t)]\,\mathrm{d}\xi_s\mathrm{d}\xi_r\mathrm{d}\omega,$$

which redefines $V_{\gamma';\gamma_0}(z_{m-1})=\langle\psi_{\gamma'},V_{\gamma_0}(z_{m-1},.,.,.)\rangle_{(s,r,t)}$ in (4.7) to obtain $\langle\psi_\gamma,\bar{F}\varphi_{\gamma_0}\rangle_{(s,r,t)}$. We have

$$V_{\gamma';\gamma_0}(z_{m-1})=[A^*_{\mathrm{WE};m-1}]_{\gamma'\gamma_0},\tag{5.7}$$

with

$$A^*_{\mathrm{WE};m-1}\ :\ r\mapsto\int_{z_{m-1}}^{z_m}H(z_{m-1},z')Q_{-,s}(z')Q_{-,r}(z')\Lambda E_3 r(z',.,.)\,\mathrm{d}z',$$

the propagation of singularities of which is described by a transformation, $\Sigma_{A;m-1}$ say [1]. This transformation provides a means, for example, to identify $(s,r,t,\xi_s,\xi_r,\omega)$ that match γ_0, that is,

$$z=z_{j0},\ s-\Delta_m\frac{\partial\Gamma}{\partial\xi_s}=r-\Delta_m\frac{\partial\Gamma}{\partial\xi_r}=x_{j0},\ t=\Delta_m\frac{\partial\Gamma}{\partial\omega},\ \frac{\xi_s-\xi_r}{2\omega}=p_{j0}$$
$$\text{and }(\xi_z,\xi_s+\xi_r,0)=2^{k_0}\nu_0\text{ with }\Gamma=\Gamma(z_m,s,r,\xi_s,\xi_r,\omega),\ \Delta_m=z-z_{m-1}.$$

Conversely, the transformation provides a means to identify (z,x,p,ν), and Δ_m, that match γ'. We note that in this process is not symmetric in s and r. We will use this identification while generating the numerical examples.

5.3. Illumination-corrected imaging and reconstruction. The "partial" redatuming step remains the same. We adapt the second step concerning the "partial" reconstruction. We have

$$\Psi_{m-1}=A_{\mathrm{WE};m-1}A^*_{\mathrm{WE};m-1}\tag{5.8}$$

[1] This transformation follows from the composition,

$$\left\{\left(s,r,t,\xi_s-\Delta_m\frac{\partial\Gamma}{\partial s},\xi_r-\Delta_m\frac{\partial\Gamma}{\partial r},t;z,s-\Delta_m\frac{\partial\Gamma}{\partial\xi_s},r-\Delta_m\frac{\partial\Gamma}{\partial\xi_r},t-\Delta_m\frac{\partial\Gamma}{\partial\omega},\Gamma,\xi_s,\xi_r,\omega\right)\right\}$$
$$\circ\left\{\left(z,s,r,\left\langle\frac{\xi_s-\xi_r}{2\omega},r-s\right\rangle,\xi_z,\xi_s,\xi_r,\omega;z,\frac{s+r}{2},\frac{\xi_s-\xi_r}{2\omega},\xi_z,\xi_s+\xi_r,(r-s)\omega\right)\right\}.$$

with principal symbol given in [38, Proposition 3.2]. In analogy with (4.20), the "partial" reconstruction is accomplished by solving

$$\widetilde{D}_\Psi(z_{m_0-1})^{-1}[A_{\mathrm{WE};m_0-1}]\Pi^{\mathcal{S}(z_{m_0-1})}[A^*_{\mathrm{WE};m_0-1}]\Pi^{\mathcal{C}(z_{m_0-1})}(r) = \widetilde{D}_\Psi(z_{m_0-1})^{-1}[A_{\mathrm{WE};m_0-1}]\Pi^{\mathcal{S}(z_{m_0-1})}(d(z_{m_0-1})) \tag{5.9}$$

for (r) upon substituting for $(d(z_{m_0-1}))$ the solution of (4.17), where

$$\widetilde{D}_\Psi(z_{m-1})^{-1}[A_{\mathrm{WE};m-1}]\Pi^{\mathcal{S}(z_{m-1})}[A^*_{\mathrm{WE};m-1}]\Pi^{\mathcal{C}(z_{m-1})} \approx \widetilde{D}_\Psi(z_{m-1})^{-1}[\Psi_{m-1}]\Pi^{\mathcal{C}(z_{m-1})} \approx \Pi^{\mathcal{C}(z_{m-1})}.$$

Now, $\mathcal{C}(z_{m-1}) \subset \Sigma^{-1}_{A;m-1}(\mathcal{S}(z_{m-1}))$.

6. Numerical example. The common component in the diffraction and reflection formulation for illumination analysis is the correction with $\widetilde{D}_{\gamma'}(z_{m-1})$. We illustrate this diagonal matrix by computing $\sum_{\bar{\gamma}'}[A^{\mathcal{S}}(z_{\bar{m}-1}, z_{m-1})]_{\bar{\gamma}'\gamma'}\psi_{\bar{\gamma}'}$, in particular at $\bar{m} = m$, and assessing how well the underlying matrix is approximated by its diagonal.

As the background (c_0) we use the low velocity lens model depicted in Fig. 2; the dot in this figure indicates the scattering point position, (z, x), common in the subsequent numerical examples, and the dashed line indicates the chosen value of z_{m-1}. The lens is responsible for the formation of caustics. The local reflector dips $((\xi_z, \xi_x)/\|(\xi_z, \xi_x)\|)$ and scattering angles (corresponding with p) considered are indicated by the arrow patterns inside the three boxes at the bottom; we let $k_0 = 1$.

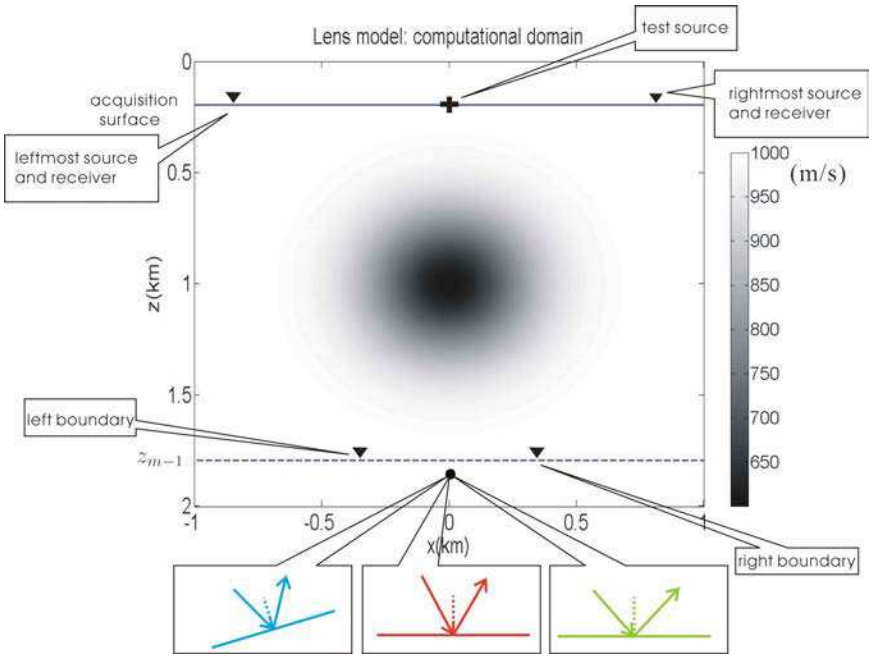

FIG. 2. *Velocity model with low-velocity lens, acquisition surface and illumination depth, z_{m-1}. A local reflector is inserted at the dot below the lens. We consider three cases with different dips and scattering angles indicated within the boxes at the bottom.*

We begin with generating the $\varphi_{\gamma'}$'s at depth z_{m-1} indicated by the dashed line in Fig. 2, locally, for subsurface sources and receivers in the between the solid triangles; they are plotted in Figs. 3 (top), 4 (top) and 5 (top). We then compute $\sum_{\bar{\gamma}'}[A^{\mathcal{S}}(z_{\bar{m}-1}, z_{m-1})]_{\bar{\gamma}'\gamma'}\psi_{\bar{\gamma}'}$, where $\mathcal{S}$ is implied by the limited acquisition geometry indicated by the solid triangles on the acquisition surface in Fig. 2.

The results, representing our illumination analysis, are illustrated in Figs. 3 (bottom), 4 (bottom) and 5 (bottom). We also computed $\sum_{\tilde{\gamma},\gamma''}[Q^*_{-,s}(0)Q^*_{-,r}(0)]_{\tilde{\gamma}\gamma''}[H(0,z_{m-1})]_{\gamma''\gamma'}\varphi_{\tilde{\gamma}}$ for a test source location (indicated by a + in Fig. 2), see Fig. 6. We observe the expected localization property (from subsurface to surface) of curvelets in phase space; for comparison, we also simulated the full synthetic data for the zero dip case (top left).

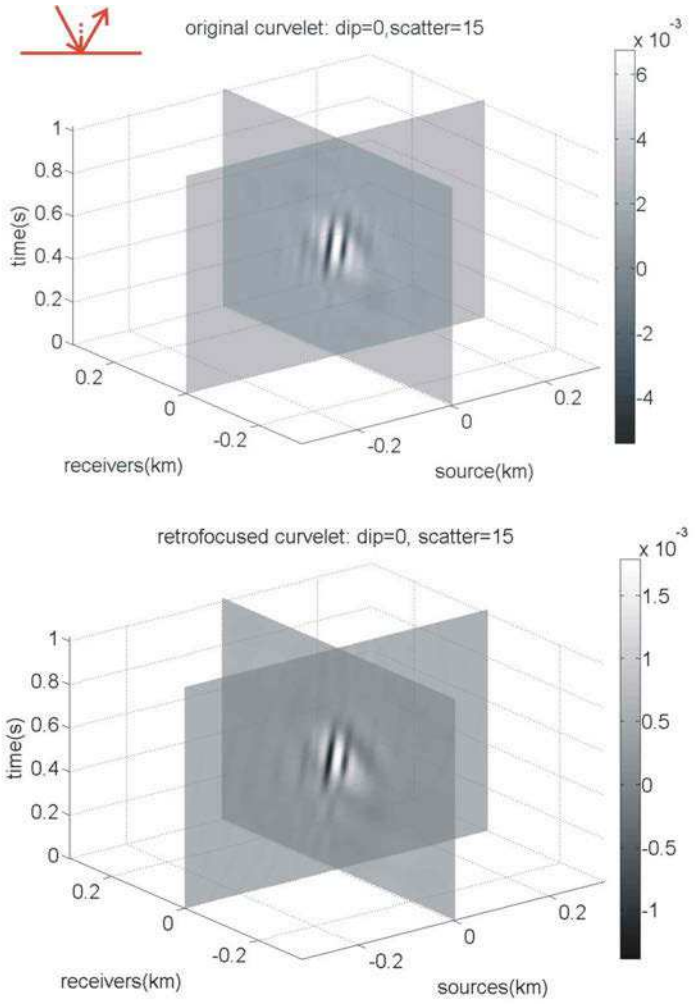

FIG. 3. *Original subsurface data curvelet (top, $n = 2$, $k' = 2$) – corresponding with zero dip (horizontal reflector) and 15° scattering angle – and retrofocused subsurface data (bottom). The subsurface data curvelet was inserted, at depth z_{m-1} (dashed line), with a source-receiver range indicated by the two triangles in Fig. 2. The surface data were restricted to a source-receiver range indicated by the two trangles on the acquisition surface in Fig. 2; most energy was captured by this acquisition geometry.*

Finally, we visualize the decay of $[A^{\mathcal{S}}(z_{m-1},z_{m-1})]_{\bar{\gamma}'\gamma'}$ away from its diagonal. We take the value of γ' corresponding with the curvelet in Fig. 3 (top). In Fig. 7 we plot, at scale $k' = 2$, the values of $|[A^{\mathcal{S}}(z_{m-1},z_{m-1})]_{\bar{\gamma}'\gamma'}|$ if $\bar{\gamma}'$ differs from γ' by translations ($(s,r,t)_{\bar{j}'} \neq (s,r,t)_{j'}$) or rotations ($\bar{\nu}' \neq \nu'$). This provides a quantification of accuracy implying whether iterations are needed for the illumination correction beyond the inverse diagonal approximation.

7. Conclusion. We have developed a technique to compensate for illumination effects in the framework of wave-equation migration. We constructed amplitude "corrections" that account for limited acquisition aperture (illumination) and that compensate for the so-called normal operator

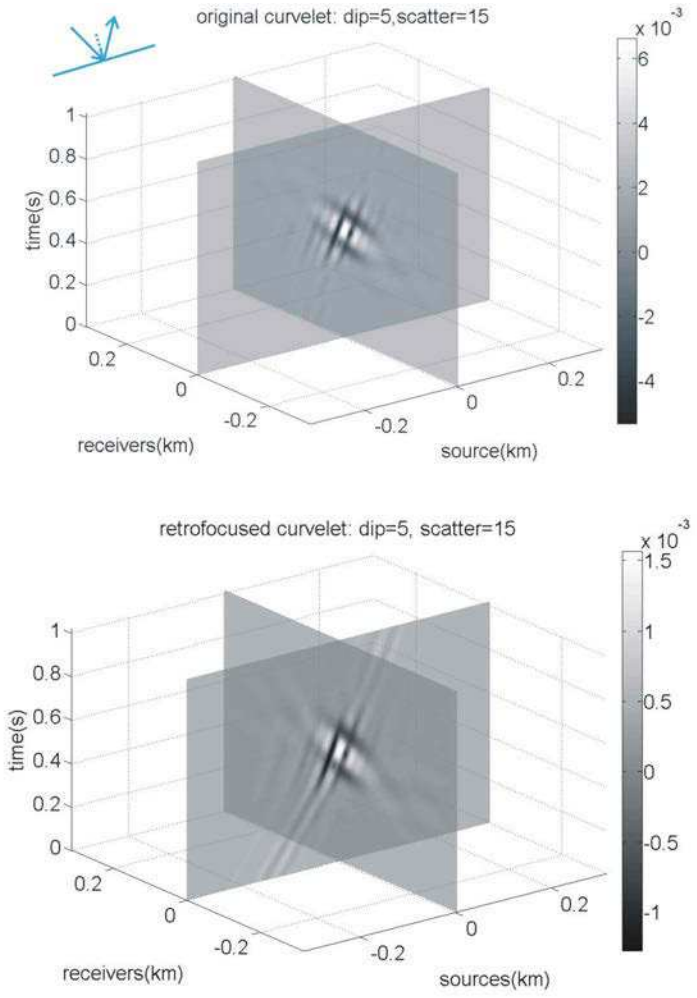

FIG. 4. *Original subsurface data curvelet (top) – corresponding with* 5^o *dip (tilted reflector) and* 15^o *scattering angle – and retrofocused subsurface data (bottom). The subsurface data curvelet was inserted, at depth* z_{m-1} *(dashed line), with a source-receiver range indicated by the two triangles in Fig. 2. The surface data were restricted to a source-receiver range indicated by the two trangles on the acquisition surface in Fig. 2; most energy was captured by this acquisition geometry.*

to yield a "true-amplitude" image of reflectivity or local reflection coefficient, while minimizing distortions and artifacts. The corrections are nested while the most significant correction is typically the one associated with the limited acquisition aperture.

The technique is based on multi-scale representations of the time-domain reflected-wave field and reflectivity in terms of curvelets. These representations can be directly connected to the propagator for downward continuation. In another paper, we discuss how the propagator, via a decomposition into curvelets, can be represented in terms of convolutions and multiplications. Moreover, the data can be compressed, and regularized, through their curvelet representations. The illumination correction can be expressed in terms of a(n infinite) matrix (with respect to curvelets) that admits an inverse via diagonal approximation; the accuracy of the diagonal approximation improves with scale as $2^{-k/2}$, k denoting dyadic scale. The same applies to the correction for the mentioned normal operator.

Curvelets can be viewed as localized "fat" plane waves. Using this viewpoint, we establish a relationship with Fourier-transform-based geophysical diffraction tomography. We decompose the

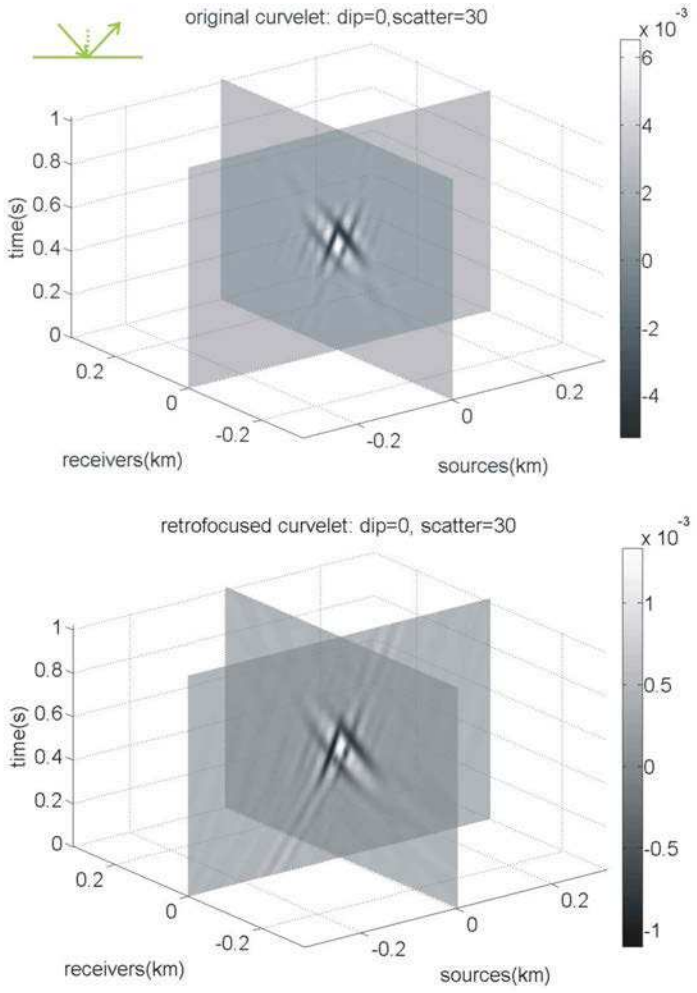

FIG. 5. *Original subsurface data curvelet (top) – corresponding with zero dip (horizontal reflector) and* 30° *scattering angle – and retrofocused subsurface data (bottom). The subsurface data curvelet was inserted, at depth* z_{m-1} *(dashed line), with a source-receiver range indicated by the two triangles in Fig. 2. The surface data were restricted to a source-receiver range indicated by the two trangles on the acquisition surface in Fig. 2; most energy was captured by this acquisition geometry.*

subsurface into thin slabs. The normal operator correction pertains to diffraction or reflection within the thin slabs, while the illumination correction pertains to downward continuation to the tops of the thin slabs. The approach presented here extends to illumination analysis within reverse-time migration. We note that the final curvelet representation of reconstructed reflectivity is amenable to carrying out regularity estimates as in [28], while paving the way for multi-scale wave-equation AVA; see also [40].

8. Acknowledgments. The authors would like to thank the members of the Geo-Mathematical Imaging Group, BP, ConocoPhillips, ExxonMobil, StatoilHydro and Total, for financial support.

Appendix A. Wave packets and curvelets.

For a non-technical introduction to curvelets, see [22]. In this section, $x \in \mathbb{R}^m$ stands for $(x, \bar{x}, t)$ ((downward-continued) data domain, $m = 2n - 1$), (z, x, p) (reflectivity domain, $m = 2n - 1$), or (z, x) (image domain, $m = n$).

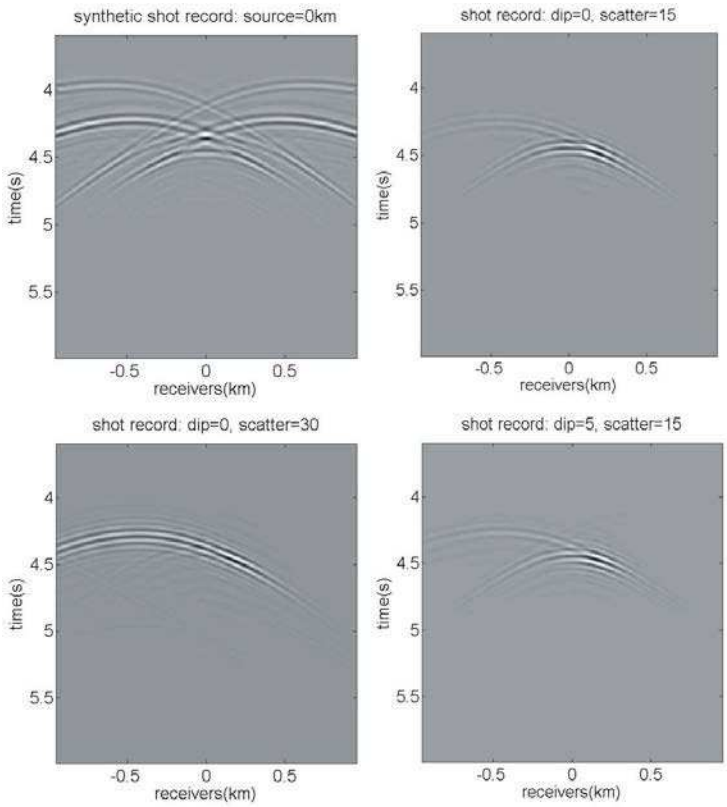

FIG. 6. *Top left: Surface data (test source position in Fig. 2) generated in the model shown in Fig. 2, while inserting a horizontal reflector through the dot below the lens. Top right: Surface data obtained by upward continuing the subsurface data curvelet shown in Fig. 3 (top). Bottom left: Surface data obtained by upward continuing the subsurface data curvelet shown in Fig. 5 (top). Bottom right: Surface data obtained by upward continuing the subsurface data curvelet shown in Fig. 4 (top). We note the localization of the latter three surface data in phase space.*

We introduce boxes (along the ξ_1-axis, that is, $\xi' = \xi_1$)

$$B_k = \left[\xi'_k - \frac{L'_k}{2}, \xi'_k + \frac{L'_k}{2}\right] \times \left[-\frac{L''_k}{2}, \frac{L''_k}{2}\right]^{m-1},$$

where the centers ξ'_k, as well as the side lengths L'_k and L''_k, satisfy the parabolic scaling condition

$$\xi'_k \sim 2^k, \quad L'_k \sim 2^k, \quad L''_k \sim 2^{k/2}, \quad \text{as } k \to \infty.$$

Next, for each $k \geq 1$, let ν vary over a set of approximately $2^{k(m-1)/2}$ uniformly distributed unit vectors. (We can index ν by $\ell = 0, \ldots, N_k - 1$, $N_k \approx \lfloor 2^{k(m-1)/2} \rfloor$: $\nu = \nu(\ell)$ while we adhere to the convention that $\nu(0) = e_1$ aligns with the ξ_1-axis.) Let $\Theta_{\nu,k}$ denote a choice of rotation matrix which maps ν to e_1, and

$$B_{\nu,k} = \Theta_{\nu,k}^{-1} B_k.$$

In the (co-)frame construction, we have two sequences of smooth functions, $\hat{\chi}_{\nu,k}$ and $\hat{\beta}_{\nu,k}$, on $\mathbb{R}^m$, each supported in $B_{\nu,k}$, so that they form a co-partition of unity

$$\hat{\chi}_0(\xi)\hat{\beta}_0(\xi) + \sum_{k \geq 1} \sum_{\nu} \hat{\chi}_{\nu,k}(\xi)\hat{\beta}_{\nu,k}(\xi) = 1, \tag{A.1}$$

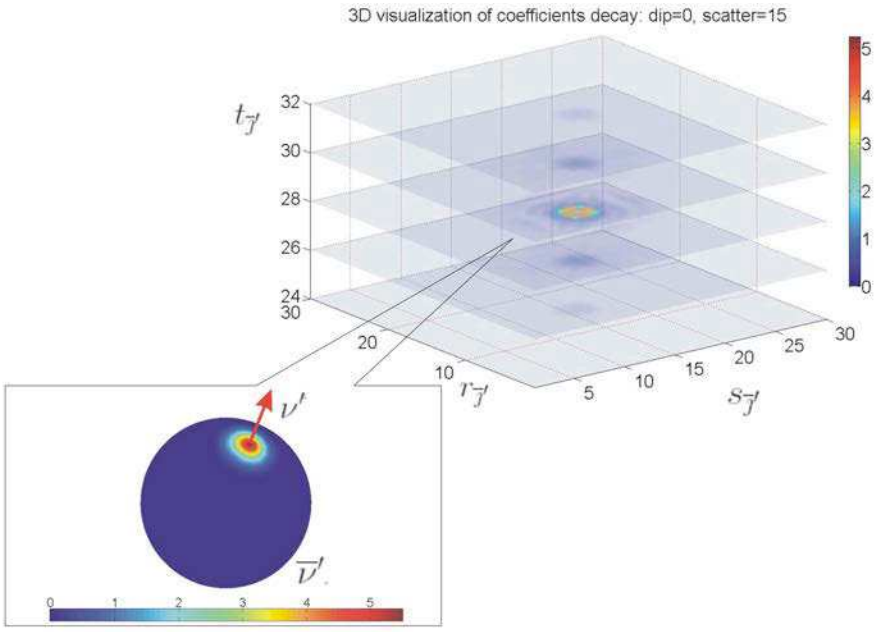

FIG. 7. *Visualization of the decay of* $[A^{\mathcal{S}}(z_{m-1}, z_{m-1})]_{\bar{\gamma}'\gamma'}$ *away from its diagonal. Here, the value of* γ' *corresponds with the curvelet in Fig. 3 (top). The values of* $|[A^{\mathcal{S}}(z_{m-1}, z_{m-1})]_{\bar{\gamma}'\gamma'}|$ *are plotted if* $\bar{\gamma}'$ *differs from* γ' *by translations* $((s,r,t)_{\bar{\jmath}'} \neq (s,r,t)_{j'})$ *or rotations* $(\bar{\nu}' \neq \nu')$.

and satisfy the estimates

$$|\langle \nu, \partial_\xi \rangle^j \, \partial_\xi^\alpha \hat{\chi}_{\nu,k}(\xi)| + |\langle \nu, \partial_\xi \rangle^j \, \partial_\xi^\alpha \hat{\beta}_{\nu,k}(\xi)| \leq C_{j,\alpha} \, 2^{-k(j+|\alpha|/2)}.$$

We then form

$$\hat{\psi}_{\nu,k}(\xi) = \rho_k^{-1/2} \hat{\beta}_{\nu,k}(\xi)\,, \quad \hat{\varphi}_{\nu,k}(\xi) = \rho_k^{-1/2} \hat{\chi}_{\nu,k}(\xi), \tag{A.2}$$

with ρ_k the volume of B_k. These functions satisfy the estimates

$$\left. \begin{matrix} |\varphi_{\nu,k}(x)| \\ |\psi_{\nu,k}(x)| \end{matrix} \right\} \leq C_N 2^{k(m+1)/4} \, (\, 2^k |\langle \nu, x \rangle| + 2^{k/2} \|x\| \,)^{-N} \tag{A.3}$$

for all N. To obtain a (co-)frame, one introduces the integer lattice: $X_j := (j_1, \ldots, j_m)$, the dilation matrix

$$D_k = \frac{1}{2\pi} \begin{pmatrix} L_k' & 0_{1\times m-1} \\ 0_{n-1\times 1} & L_k'' I_{m-1} \end{pmatrix}, \qquad \det D_k = (2\pi)^{-m} \rho_k,$$

and points $x_j = \Theta_{\nu,k}^{-1} D_k^{-1} X_j$, which change with (ν, k). The frame elements ($k \geq 1$) are then defined in the Fourier domain as

$$\hat{\varphi}_\gamma(\xi) = \rho_k^{-1/2} \hat{\chi}_{\nu,k}(\xi) \, \exp[-\mathrm{i}\langle x_j, \xi \rangle], \quad \gamma = (x_j, \nu, k), \tag{A.4}$$

and similarly for $\hat{\psi}_\gamma(\xi)$. We obtain the transform pair

$$v_\gamma = \int v(x) \overline{\psi_\gamma(x)} \, \mathrm{d}x, \qquad v(x) = \sum_\gamma v_\gamma \varphi_\gamma(x) \tag{A.5}$$

with the property that $\sum_{\gamma':\ k'=k,\ \nu'=\nu} v_{\gamma'}\hat{\varphi}_{\gamma'}(\xi) = \hat{v}(\xi)\hat{\beta}_{\nu,k}(\xi)\hat{\chi}_{\nu,k}(\xi)$, for each ν, k.

We introduce the notation C for the curvelet transform (analysis): $v_\gamma = (\mathrm{C}v)_\gamma$, and also define $\mathrm{C}^{-1}\{c_\gamma\} = \sum_\gamma c_\gamma\varphi_\gamma$ for the inverse transform (synthesis). We observe that $\mathrm{C}^{-1}\mathrm{C} = I$ on $L^2(\mathbb{R}^m)$, and that $\mathrm{C}\mathrm{C}^{-1} \equiv \Pi$ is a (not necessarily orthogonal) projection operator of ℓ^2_γ onto the range of the analysis operator C. It holds that $\Pi^2 = \Pi$, but Π is generally not self-adjoint unless $\psi_\gamma = \varphi_\gamma$. Observe that, as a matrix on ℓ^2_γ,

$$\Pi_{\gamma'\gamma} = \langle\psi_{\gamma'}, \varphi_\gamma\rangle.$$

If $A : L^2(\mathbb{R}^m) \to L^2(\mathbb{R}^m)$, then the associated matrix defined as $[A] = \mathrm{C}A\mathrm{C}^{-1}$, preserves the range of C, since $\mathrm{C}^{-1}\Pi = \mathrm{C}^{-1}$, and $\Pi\mathrm{C} = \mathrm{C}$. In particular, $[A]\Pi = \Pi[A] = [A]$.

Finally, let d denote the pseudodistance on $S^*(X)$ introduced in (Smith, Definition 2.1)

$$d(x,\nu;x',\nu') = |\langle\nu, x-x'\rangle| + |\langle\nu', x-x'\rangle| + \min\{\|x-x'\|, \|x-x'\|^2\} + \|\nu-\nu'\|^2.$$

If $\gamma = (x,\nu,k)$ and $\gamma' = (x',\nu',k')$, we define

$$\overline{d}(\gamma;\gamma') = 2^{-\min(k,k')} + d(x,\nu;x',\nu'). \tag{A.6}$$

REFERENCES

[1] R. Alai and J. Thorbecke, *Illumination of the subsurface towards identifying shadow zones and optimizing target images*, in Expanded Abstracts, Society of Exploration Geophysicists, 2008, p. 193.

[2] F. Andersson, M. Carlsson, and M.V. de Hoop, *Nonlinear approximation of functions by sums of wave packets*, Applied and Computational Harmonic Analysis, submitted (2008).

[3] F. Andersson, M.V. de Hoop, H.F. Smith, and G. Uhlmann, *A multi-scale approach to hyperbolic evolution equations with limited smoothness*, Communications in Partial Differential Equations, 33 (2008), pp. 988–1017.

[4] M.A. Ayzenberg, A.M. Aizenberg, H.B. Helle, K.D. Klem-Musatov, J. Pajchel, and B. Ursin, *3d diffraction modelling of singly scattered acoustic wavefields based on the combination of surface integral propagators and transmission operators*, Geophysics, 72 (2007), pp. SM19–SM34.

[5] G. Bear, C. Liu, R. Lu, and D. Willen, *The construction of subsurface illumination and amplitude maps via ray tracing*, The Leading Edge, 19 (2000), pp. 726–728.

[6] V. Brytik, M.V. de Hoop, and M. Salo, *Sensitivity analysis of wave-equation tomography: A multi-scale approach*, J. Four. Anal. Appl., submitted (2008).

[7] E.J. Candès and L. Demanet, *The curvelet representation of wave propagators is optimally sparse*, Communications on Pure and Applied Mathematics, 58 (2005), pp. 1472–1528.

[8] E.J. Candès, L. Demanet, D. Donoho, and L. Ying, *Fast discrete curvelet transforms*, SIAM Multiscale Model. Simul., 5-3 (2006), pp. 861–899.

[9] E.J. Candès and D. Donoho, *New tight frames of curvelets and optimal representations of objects with piecewise-C^2 singularities*, Communications on Pure and Applied Mathematics, 57 (2004), pp. 219–266.

[10] ———, *Continuous curvelet transform: I. Resolution of the wavefront set*, Applied and Computational Harmonic Analysis, 19 (2005), pp. 162–197.

[11] E.J. Candès and D. Donoho, *Continuous curvelet transform: II. Discretization and frames*, Applied and Computational Harmonic Analysis, 19 (2005), pp. 198–222.

[12] H. Chauris and T. Nguyen, *Seismic demigration/migration in the curvelet domain*, Geophysics, 73 (2008), pp. S35–S46.

[13] L. Chen, R.-S. Wu, and Y. Chen, *Beamlet migration based on gabor-daubechies frame decomposition*, Geophysics, 71 (2006), pp. S37–S52.

[14] M.L. Clapp, R.G. Clapp, and B. Biondi, *Regularized least-squares inversion for 3-d subsalt imaging*, in Expanded Abstracts, Society of Exploration Geophysicists, 2005, p. 1814.

[15] C.G.M. de Bruin, C.P.A. Wapenaar, and A.J. Berkhout, *Angle-dependent reflectivity by means of prestack migration*, Geophysics, 55 (1990), pp. 1223–1234.

[16] M.V. de Hoop, *Generalization of the bremmer coupling series*, J. Math. Phys., 37 (1996), pp. 3246–3282.

[17] M.V. de Hoop, J.H. Le Rousseau, and B.L. Biondi, *Symplectic structure of wave-equation imaging: A path-integral approach based on the double-square-root equation*, Geophys. J. Int., 153 (2003), pp. 52–74.

[18] M.V. de Hoop, J.H. Le Rousseau, and R.-S. Wu, *Generalization of the phase-screen approximation for the scattering of acoustic waves*, Wave Motion, 31 (2000), pp. 43–70.

[19] M.V. de Hoop, H.F. Smith, G. Uhlmann, and R.D. van der Hilst, *Seismic imaging with the generalized radon transform: A curvelet transform perspective*, Inverse Problems, 25 (2009), pp. doi:10.1088/0266–5611/25/2/025005.

[20] M.V. De Hoop, C. Spencer, and R. Burridge, *The resolving power of seismic amplitude data: An anisotropic inversion/migration approach*, Geophysics, 64 (1999), pp. 852–873.
[21] A.J. Devaney, *Geophysical diffraction tomography*, IEEE Trans. Geosc. and Rem. Sens., GE-22 (1984), pp. 3–13.
[22] H. Douma and M.V. De Hoop, *Leading-order seismic imaging using curvelets*, Geophysics, 72 (2007), pp. S231–S248.
[23] A.A. Duchkov, F. Andersson, and M.V. De Hoop, *Discrete, almost symmetric wave packets and multi-scale geometric representation of (seismic) waves*, Journal of Computational Physics, submitted (2008).
[24] A.A. Duchkov, M.V. De Hoop, and A.S. Sá Barreto, *Evolution-equation approach to seismic image, and data, continuation*, Wave Motion, 45 (2008), pp. 952–969.
[25] L.J. Gelius, I. Lecomte, and H. Tabti, *Analysis of the resolution function in seismic prestack depth imaging*, Geophysical Prospecting, 50 (2002), pp. 505–515.
[26] H. Kühl and M.D. Sacchi, *Least-squares wave-equation migration for avp/ava inversion*, Geophysics, 68 (2003), pp. 262–273.
[27] J.H. Le Rousseau, *Fourier-integral-operator approximation of solutions to first-order hyperbolic pseudodifferential equations i: Convergence in sobolev spaces*, Communications in Partial Differential Equations, 31 (2006), pp. 867–906.
[28] C.L. Li, C.-F.and Liner, *Wavelet-based detection of singularities in acoustic impedance from surface reflection data*, Geophysics, 73 (2008), pp. V1–V9.
[29] M. Luo, J. Cao, X.-B. Xie, and R.-S. Wu, *Comparison of illumination analyses using one-way and full-wave propagators*, in Expanded Abstracts, Society of Exploration Geophysicists, 2004, p. 67.
[30] D. Muerdter, M. Kelly, and D. Ratcliff, *Understanding subsalt illumination through ray-trace modeling, part 2: Dipping salt bodies, salt peaks, and nonreciprocity of subsalt amplitude response*, The Leading Edge, 20 (2001), pp. 688–697.
[31] D. Muerdter and D. Ratcliff, *Understanding subsalt illumination through ray-trace modeling, part 1: Simple 2-d salt models*, The Leading Edge, 20 (2001), pp. 578–594.
[32] ———, *Understanding subsalt illumination through ray-trace modeling, part 3: Salt ridges and furrows, and the impact of acquisition orientation*, The Leading Edge, 20 (2001), pp. 803–816.
[33] J.E. Rickett, *Illumination-based normalization for wave-equation depth migration*, Geophysics, 68 (2003), pp. 1371–1379.
[34] W.E.A. Rietveld and A.J. Berkhout, *Prestack depth migration by means of controlled illumination*, Geophysics, 59 (1994), pp. 801–809.
[35] H.F. Smith, *A parametrix construction for wave equations with $C^{1,1}$ coefficients*, Ann. Inst. Fourier, Grenoble, 48 (1998), pp. 797–835.
[36] C.C. Stolk, *A pseudodifferential equation with damping for one-way wave propagation in inhomogeneous acoustic media*, Wave Motion, 40 (2004), pp. 111–121.
[37] C.C. Stolk and M.V. De Hoop, *Modeling of seismic data in the downward continuation approach*, SIAM Journal on Applied Mathematics, 65 (2005), pp. 1388–1406.
[38] ———, *Seismic inverse scattering in the downward continuation approach*, Wave Motion, 43 (2006), pp. 579–598.
[39] W.W. Symes, *Approximate linearized inversion by optimal scaling of prestack depth migration*, Geophysics, 73 (2008), pp. R23–R35.
[40] C.P.A. Wapenaar, *Seismic reflection and transmission coefficients of a self-similar interface*, Geophys. J. Int., 135 (1998), pp. 585–594.
[41] R.-S. Wu and L. Chen, *Directional illumination analysis using beamlet decomposition and propagation*, Geophysics, 71 (2006), pp. S147–S159.
[42] R.-S. Wu and M.N. Toksöz, *Diffraction tomography and multisource holography applied to seismic imaging*, Geophysics, 52 (1987), pp. 11–25.
[43] X.-B. Xie, S. Jin, and R.-S. Wu, *Wave-equation-based seismic illumination analysis*, Geophysics, 71 (2006), pp. S169–S177.